International Journal for Computational Civil and Structural Engineering, 20(3) 56–68 (2024)

DOI:10.22337/2587-9618-2024-20-3-56-68

NONLINEAR DYNAMIC ANALYSIS OF WIND ACTIONS ON A CABLE-STAYED GLASS FAÇADE SYSTEM

Oleg S. Goryachevsky, Alexander M. Belostotsky

National Research Moscow State University of Civil Engineering, Moscow, RUSSIA

Abstract: This paper presents the results of a nonlinear dynamic analysis of wind actions on a cable-stayed glass façade. The wind impact was determined by a transient eddy-resolving numerical simulation using a hybrid RANS-LES model SBES. The revealed dynamic response of the façade system confirms the relevance of dynamic calculations compared to simplified static approaches.

Keywords: computational fluid dynamics (CFD), wind action, wind response, cable-stayed glass façade system, nonlinear dynamic analysis

НЕЛИНЕЙНЫЙ ДИНАМИЧЕСКИЙ РАСЧЕТ ВАНТОВОГО СВЕТОПРОЗРАЧНОГО ФАСАДА НА ВЕТРОВЫЕ ВОЗДЕЙСТВИЯ

О.С. Горячевский, А.М. Белостоцкий

Национальный исследовательский Московский государственный строительный университет, г. Москва, РОССИЯ

Аннотация: В статье представлены результаты нелинейного динамического расчета вантового светопрозрачного фасада на ветровое воздействие. Ветровое воздействие было определено в результате численного моделирования в нестационарной вихреразрешающей постановке по гибридной модели SBES. Выявленный динамический отклик фасадной системы подтверждает актуальность динамических расчетов по сравнению с упрощенными статическими подходами.

Ключевые слова: вычислительная гидродинамика, ветровое воздействие, отклик на ветровое воздействие, вантовый светопрозрачный фасад, нелинейный динамический анализ

1. INTRODUCTION

The widespread use of complex and costly façade systems in modern construction challenges engineers to correctly calculate their robustness, stiffness and stability. The situation becomes even more complicated if the façade structures are flexible (possessing low eigenfrequencies) and their mechanical behaviour is significantly non-linear; for instance, cable-stayed glass façades (CSGF), Fig. 1.

As a rule, wind loads are the most important for façade structures. Physical modelling utilising wind tunnels (PM) is currently the most common and well-studied method for determining wind loads for non-typical structures. Along with its advantages, PM has a number of disadvantages, among which are the reduced scale of the models, limited consideration of the surrounding buildings and terrain, measurement of the required parameters in a small number of points (usually a few dozen).

In the last 30 years, interest in numerical modelling of wind loads (NM) has grown significantly [1,2]. NM has almost unlimited possibilities to take into account surrounding buildings, topography, climatic effects and a number of other factors, allows obtaining results in millions of points, processing and visualising

them freely. High computational complexity and use of simplifying hypotheses that reduce accuracy have for a long time restrained the introduction of NM in construction practice [3,4]. However, the development of computational techniques, turbulence models, numerical methods and software currently allows full use of NM as a tool for determining wind actions [5,6]. Today, NM is implemented in foreign [7,8] and Russian regulatory documents [9,10], and is actively used in many construction companies.

(a) exterior view

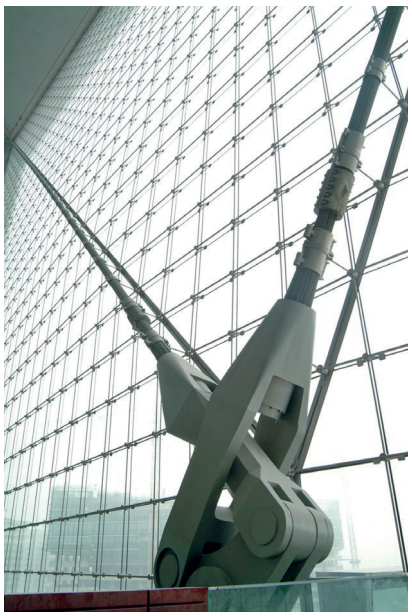

(b) interior view

Figure 1. Beijing Poly Plaza Hotel, China

The research on a CSGF's stress-strain state started in the 2000s. Let us highlight the main ones in chronological order (2009-2023).

In [11], Feng et al. found that glazing elements increase the façade stiffness up to 30% and the damping performance from 0.1% to 3.5-4.5% compared to an unglazed cable network. In [12] Feng, based on the nonlinear differential equation of vibration, analysed the response spectra to seismic load. It was found that the influence of nonlinearities decreases when the natural frequencies of vibration increase. In [13], Feng experimentally and numerically (using ANSYS Mechanical) revealed a significant difference in the glazing's stress-strain state when using spiders and clamping plates.

Amadio and Bedon investigated the potential of elastic-plastic dampers to reduce the response to blast effects on the basis of dynamic analysis [14,15]. It was found that cables are the most vulnerable to blast effects, and the use of dampers can reduce the maximum forces in them while maintaining flexures.

The most extensive study of CSGFs is done in Yussof's thesis [16]. In his work, an overview of the application, implementation and types of CSGFs is presented. A set of experimental and parametric numerical studies in Simulia ABAQUS are carried out. Static load, impact load on the glass and cable removal are considered.

In [17], Wang experimentally and numerically investigated the dynamic behaviour of CSGFs. Several first eigenfrequencies and modes, as well as damping coefficients, were determined. It was found that the sealant has almost no effect on the vibrations and can be disregarded.

The study by Xiang [18] focuses on evaluating the effect of the building load-bearing system on the response of a CSGF to seismic loading.

In 2023, numerical studies of wind actions on CSGFs in a direct dynamic formulation appeared. In [19], Rizzo used wind pressures obtained in a wind tunnel, while in [20] Zhou generated synthetic wind loads using a random Gaussian process model. Rizzo's study focused

mainly on modelling, while Zhou's study focused on finding simplified mathematical models. Zhou also showed that the behaviour of a CSGF is reliably described by thin membrane theory when the cables are dense.
Among the published studies of CSGFs, no papers were found in which wind loads were determined on the basis of NM. Thus, the choice of NM for determining wind loads determines the scientific novelty of the paper.

2. METHODOLOGY AND OBJECT

2.1 Object and task description

The object is a CSGF of an office building (Fig. 2). The building is being constructed on the territory of the new modern town of Rublevo-Arkhangelskoye in the western part of Moscow (Fig. 3).

Figure 2. Investigated Building with CSGF

Figure 3. Render of Rublevo-Arkhangelskoye

The polygonal in plan building is 122 m long, 58 m wide and 34 m tall. The maximum height of the CSGF is 19.34 m, and the minimum height is 2.99 m.
In a structural sense, the façade consists of:

- vertical pre-stressed load-bearing steel cables with a diameter of 30 mm;
- single glazing units with maximum dimensions of 2880 × 1480(h) mm and a total glass thickness of 28 mm;
- cable attachment assemblies to glass panes (spiders);
- cable attachment assemblies to reinforced concrete and steel structures.

According to SP 20.13330, the construction site is located in wind zone I (w_0 = 230 Pa), terrain type C.
Among the loads, dead weight, internal and external wind loads were taken into account. The internal wind pressure was calculated according to paragraph B.1.9 of SP 20.13330, and the external wind pressure was calculated on the basis of PM.
Cable pretension is set from 5 to 20 tf (higher in areas of maximum flexure).

The stress-strain state received was assessed according to the following criteria:

- relative flexures of cables (< 1/200 length, demanded by SP 20.13330);
- relative flexures of insulating glass units (< 1/250, which is equal to 5.92 mm, demanded by GOST 24866-2014);
- maximum forces in cables (< R_{dh} = 40.76 tf, demanded by SP 16.13330).

A computationally economical methodology was used to determine the wind loads on the façade:
1. Initially, hazardous wind directions were determined by steady-state RANS simulations (SST k-ω model);
2. For the identified hazardous wind directions, the refined values of peak wind pressures and pressure time series for each glazing element were determined based by transient simulations (using a hybrid RANS-LES model SBES).

The dynamic stress-strain state of the façade system was then analysed, taking into account cable pretension, damping and geometric nonlinearity from time-dependent wind pressures.

2.2 CFD model description

NM of the wind actions was carried out in ANSYS Fluent using the finite volume (FV) method. The geometrical model of the building is shown in Fig. 4. Different polyhexagonal meshes were used for steady-state and transient simulations (Figs. 5-6).

The modelling was carried out at a geometric scale of 1:100 (integral loads were scaled during processing).

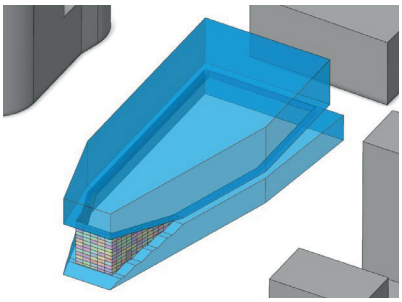

Figure 4. Calculation area near the GSCF

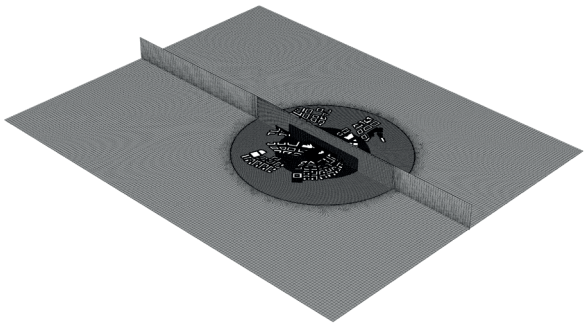

Figure 5. Mesh for RANS (10.2m cells)

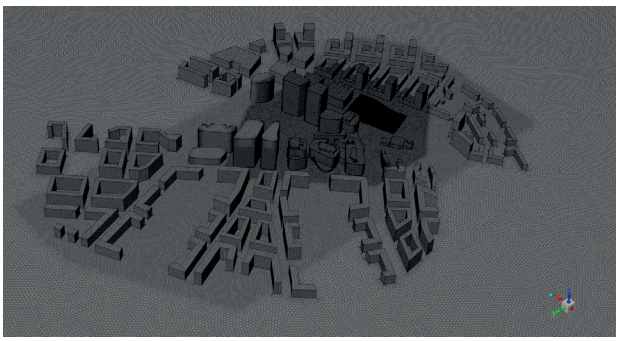

Figure 6. Mesh for SBES (9.2-9.5m cells)

Steady-state (RANS) simulations were performed using the SST k-ω turbulence model [21].

Transient simulations were performed using a hybrid RANS-LES model SBES [22]. The RANS model SST k-ω in the near-wall and vortex-free zones and the LES model WALE [23] in the other regions were coupled (mixed).

The hybrid SBES model is based on spatial mixing of turbulent viscosity:

$$\nu_t^{SBES} = f_{SDES}\nu_t^{RANS} + f_{SDES}\nu_t^{LES}, \qquad (1)$$

where ν_t^{RANS} is the turbulent viscosity of RANS models (determined by the Boussinesq hypothesis); ν_t^{LES} is the subgrid viscosity of LES models; f_{SDES} is a special function providing the transition between LES and RANS zones (shielding function).

For steady-state simulations, the Coupled pressure-velocity solver was used. For transient simulations, the segregated SIMPLEC solver was used.

Spatial numerical discretisation schemes over space were applied [24]:

- (RANS) Second Order Upwind for the momentum equation;
- (SBES) Bounded Central Differencing for the momentum equation (coefficient 0.75);
- Second Order Upwind for the turbulent transport equations;
- Second Order Upwind for the interpolation of pressures;
- Least Squares Method to calculate gradients in the centroids of FVs.

Time integration for SBES was performed using Bounded Second Order Implicit scheme. The time step $\Delta t = 0.0002$ s (physical 0.02 s).

The following boundary conditions for the computational domain were applied:

1.The velocity profile at the inlet: $U(z)$, taken from the building code;

2. Turbulence intensity 1% (total turbulence is modelled directly by the flow moving through the surrounding buildings);

3.Backflow pressure at the outlet: $\overline{p} = 0$;

4.Free slip wall conditions were set for the lateral and upper boundaries;
5.No-slip wall conditions were set for the ground and building surfaces.

2.3 Peak wind load calculation

RANS simulations were performed for 36 wind directions (in 10° increments), and transient simulations were performed only for the identified hazardous directions.
Peak wind pressures $p_{e,+(-)}$ from RANS simulations were estimated using a semi-empirical model [25]:

$$\begin{aligned} p_{e,+} &= \Delta\overline{p} + \theta_+ \sigma_p; \\ p_{e,-} &= \Delta\overline{p} - \theta_- \sigma_p; \\ \sigma_P &= \left(2I_U + I_U^2\right)\Delta\overline{p}; \end{aligned} \tag{2}$$

$$I_U = \sqrt{\frac{\rho_{air} k}{3\left|\Delta\overline{p}\right|}}, \tag{3}$$

where $\theta_+ = 0.5$, $\theta_- = 1.5$ are calibration coefficients; k is the turbulent kinetic energy near the wall, $\Delta\overline{p}$ is the mean pressure at the wall.
The accuracy of the (2-3) model is sufficient to identify the hazardous wind directions.
Based on (2-3), the peak integral wind loads on each of the 3 sides of the façade were calculated:

$$\begin{aligned} F_{n,+(-)} &= \int_S w_{e,+(-)} dS = \\ &= v_{+(-)}\left(1+\zeta\right)\int_S p_{e,+(-)} dS, \end{aligned} \tag{4}$$

where S is the area of the facade side (one of three); $\zeta = 1.31$ is wind pressure pulsation coefficient for terrain type C; $v_{+(-)} = 0.75(0.65)$ is correlation coefficient (both taken from SP 20.13330).
For RANS simulations, 450 iterations with stepwise relaxation enhancement were calculated.
Based on the results of transient simulations, integral values of peak wind loads and peak pressures on glazing elements were determined, which were further used in static calculations:

$$\begin{aligned} F_{n,+} &= \max_j \int_S \Delta p(t_j) dS; \\ F_{n,-} &= \min_j \int_S \Delta p(t_j) dS; \end{aligned} \tag{5}$$

$$w_{e,+(-)} = \frac{1}{S}\int_S \Delta p(t_k) dS; \tag{6}$$

where S is the area of the façade side / glazing element; t_j is the j-th physical timestep; t_k is the k-th timestep at which the maximum of integral forces (5) is achieved for the façade side on which the corresponding glazing element is located.
Formulas (5-6) do not contain pulsation and pressure correlation coefficients because the corresponding effects are modelled directly.
The total physical time during transient simulations was 5.2-5.7 s (~$2.7 \cdot 10^4$ time steps, real-scale 7.8-8.5 min). During the post-processing, the first 0.5 s were discarded.

2.4 FEM model description

Stress-strain state calculations of the GSCF were carried out in the ANSYS Mechanical using the following finite element types: SHELL181 (for glazing elements), LINK180 (for cables), BEAM188 (for columns, spiders and door frames), MASS21 (to simulate the mass of the non-load-bearing part of spiders and luminaires).
The total dimensionality of the finite element model (Figs. 7-8) is 57440 nodes / 52925 FEs / ~334000 variables.

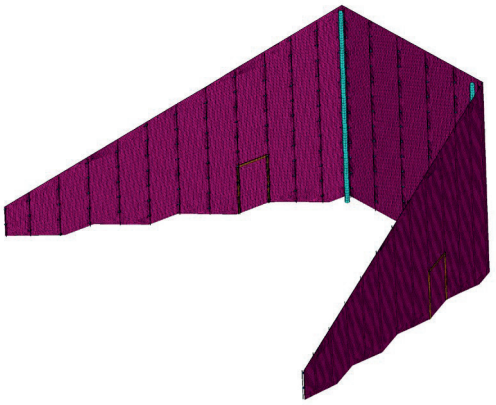

Figure 7. FEM model - general view

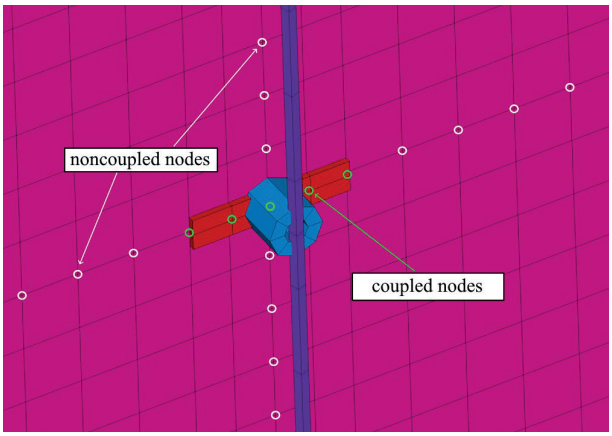

Figure 8. FEM model - cable and glass connection diagram

Columns and cables are fixed in all degrees of freedom at the points of attachment to the load-bearing structures of the building. The windows are attached using roller supports (free in the façade plane) at the upper and lower façade marks, except for the corner points of each window, which are attached using hinged supports.

All calculations were carried out in a geometrically nonlinear formulation taking into account cable pretension.

For dynamic calculations, the time step was set to $\Delta t = 0.01$ s (see Section 3.2).

Numerical Newton-Raphson method was used for resolving the nonlinearity and Newmark method was used for time integration.

Damping was accounted for by the Rayleigh hypothesis with a damping coefficient in fractions of the critical $\xi = 0.035$ [11].

3. RESULTS AND DISCUSSION

3.1 Peak wind load results

The analysis of peak values of integral loads (Fig. 9) obtained from the static simulations revealed 4 hazardous wind directions: 130°, 200°, 230° and 310°. For each of these directions, a refined transient simulation was carried out (Table 1).

It should be clarified that the loads given in Table 1 do not take into account the dynamic response of the structure.

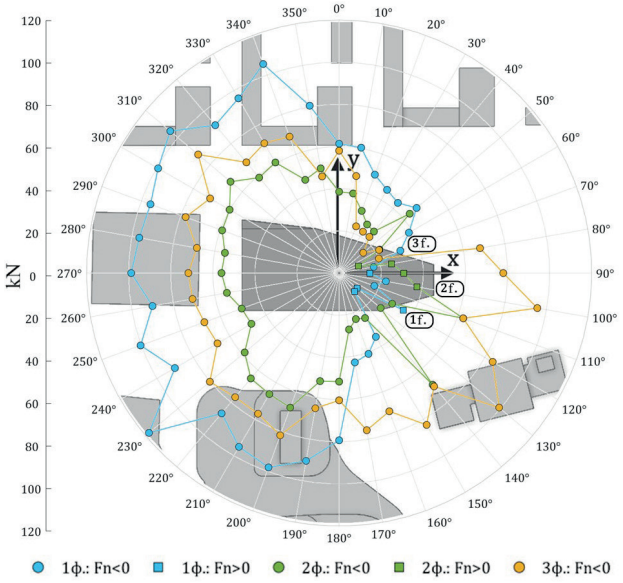

Figure 9. Pie chart of F_n [kN] obtained in the steady simulations

Table 1. Peak wind loads on the façade sides

Wind attack angle, °	Simulation	F_n, kN		
		1f.	2f.	3f.
130	SST	55.1	-25.8	-99.3
	SBES	54.8	-64.5	-105
200	SST	-98.1	-67.9	-81.9
	SBES	-66.8	-69.8	-71.0
230	SST	-118.0	-58.6	-80.2
	SBES	-70.5	-52.3	-69.0
310	SST	-105	-67.4	-87.4
	SBES	-75.2	-54.2	-60.9

Examples of the resulting time series and spectra are shown in Figs. 10-13.

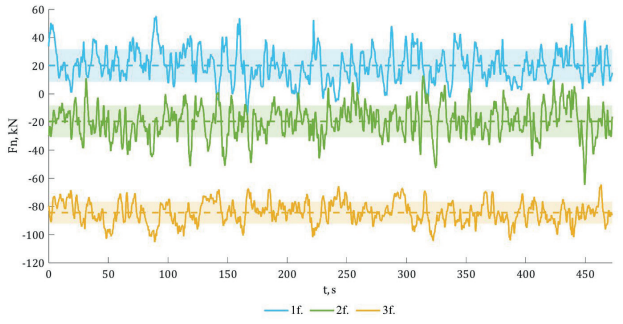

Figure 10. Steady-state fluctuations of integral wind loads on the facade sides, kN (130°)

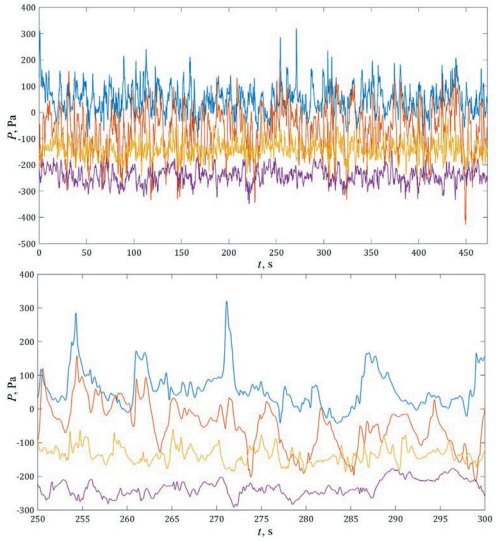

Figure 11. Steady-state wind pressure fluctuations for 4 characteristic glazing elements, Pa (130°)

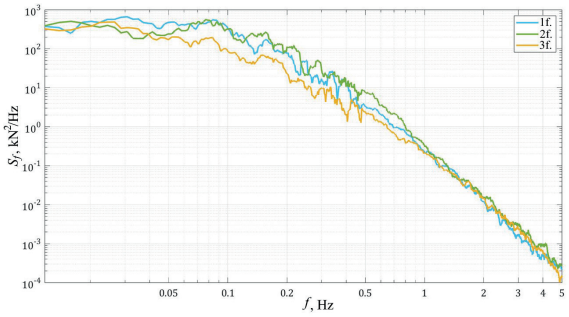

Figure 12. Power spectral power density of integral wind loads on facade sides, kN^2 /Hz (130°)

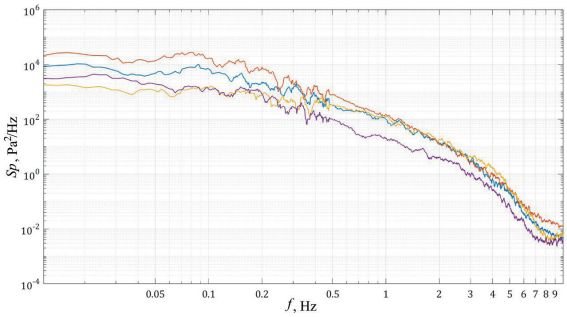

Figure 13. Pressure power spectral power density for 4 characteristic glazing elements, Pa^2 /Hz (130°)

Analysis of the peak integral wind loads show that the wind loads obtained through the transient simulations may differ significantly from the RANS approach.

Analysis of time series and spectra of wind loads shows significant fluctuations of wind loads in a wide frequency range. This corresponds to the physical nature of the phenomenon and can potentially lead to resonant vibrations of flexible structures.

Examples of velocity and pressure distributions in a horizontal section at a height of 15 m are shown in Figs. 14-15. Fig. 16 shows the pressure distributions over the façade surface.

(a) SST: $\overline{V}$

(b) SBES: $\overline{V}$

(c) SBES: σ_V

(d) SBES: $V(t_i)$

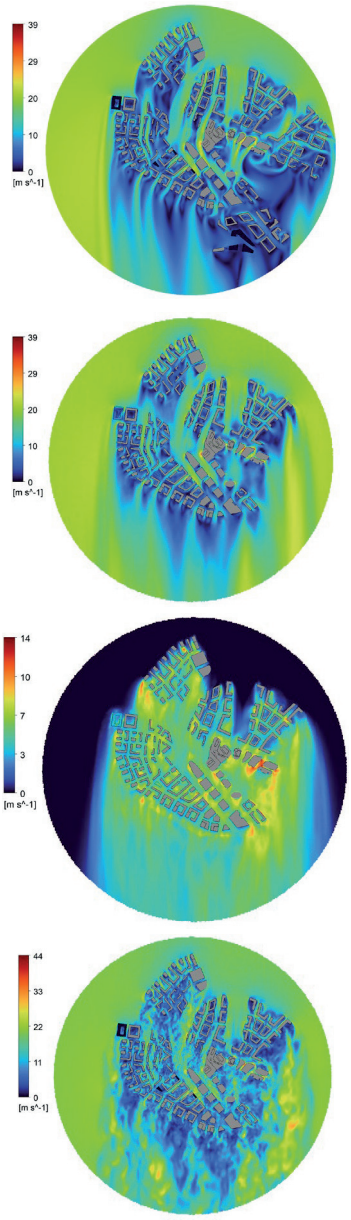

Figure 14. Instantaneous, mean and standard deviation values of velocity [m/s] in horizontal section, 130°

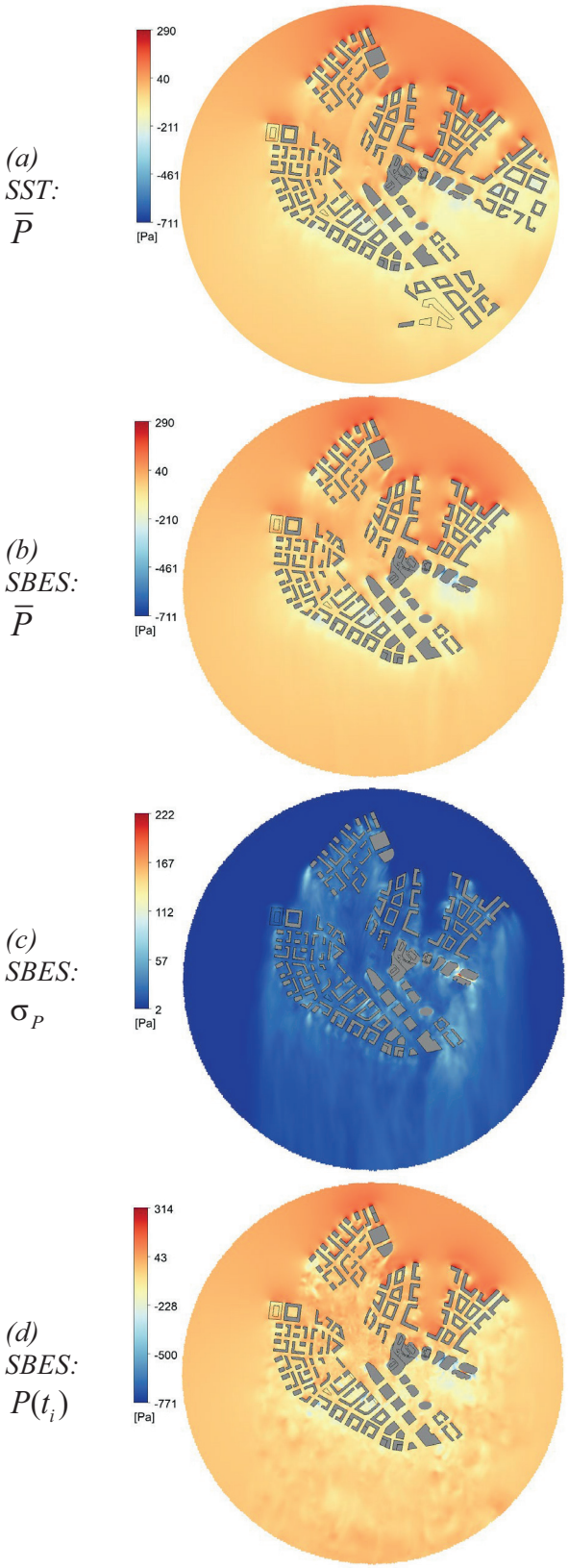

Figure 15. Instantaneous, mean and standard deviation values of pressure [Pa] in horizontal section, 130°

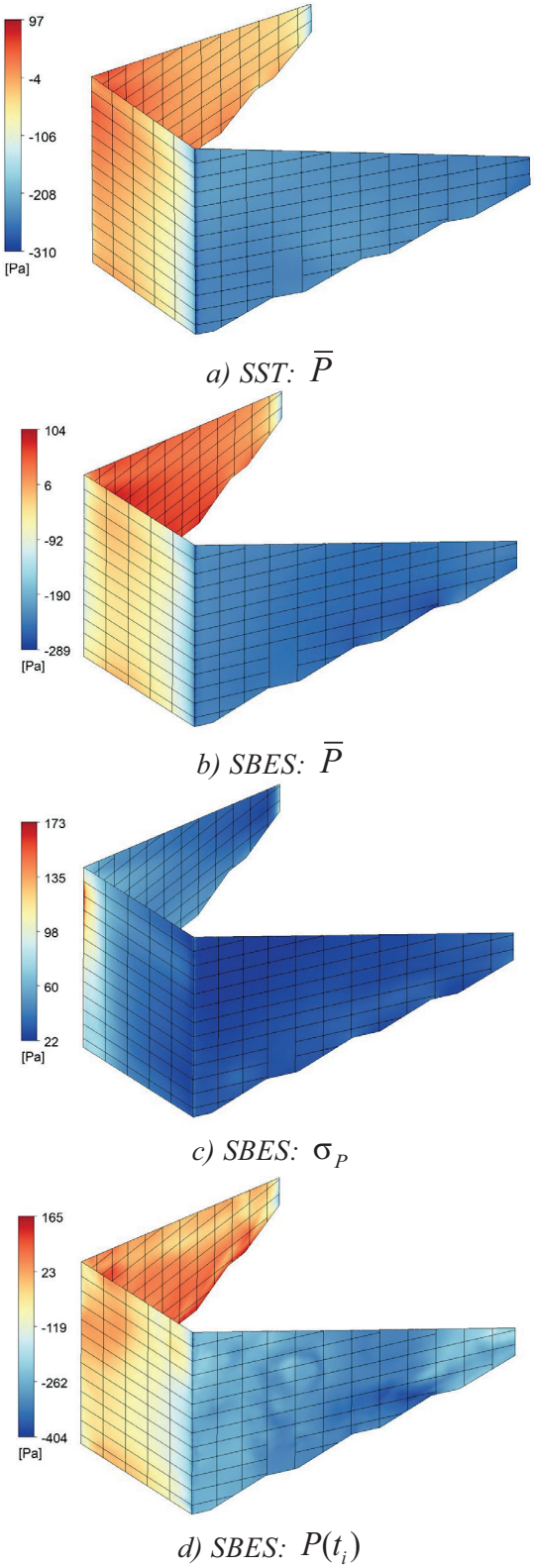

Figure 16. Instantaneous, mean and standard deviation values of pressure [Pa] on the façade surface, 130°

3.2 Modal analysis results

To determine the time step required for transient calculations, the modes and eigenfrequencies were initially analysed (Fig. 17).

Starting from 18 Hz, only the highest modes of individual glazing elements are observed, and it makes no practical sense to take them into account. Therefore, the timestep $\Delta t = 0.01$ s is chosen, which corresponds to ~6 steps for the smallest considered eigenfrequency (1/18.0 Hz = 0.056 s, 308th form)

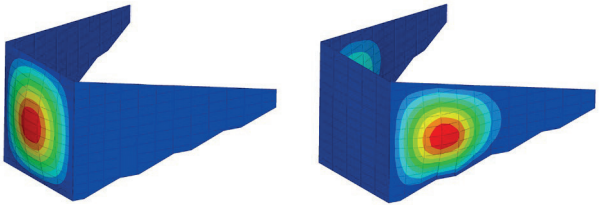

(a) f_1 = 1.053 Hz *(b) f_2 = 1.178 Hz*

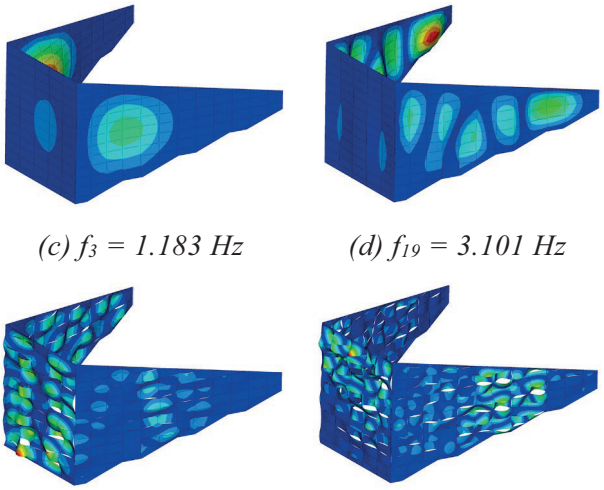

(c) f_3 = 1.183 Hz *(d) f_{19} = 3.101 Hz*

(d) f_{117} = 10.026 Hz *(e) f_{308} = 18.049 Hz*

Figure 17. Characteristic frequencies and modes

3.3 Stress-strain state results

Figs. 18-20 show the maximum values of the flexures of the glazing elements and cables and the forces in the cables over time. Figs. 21-23 show corresponding examples of time series.

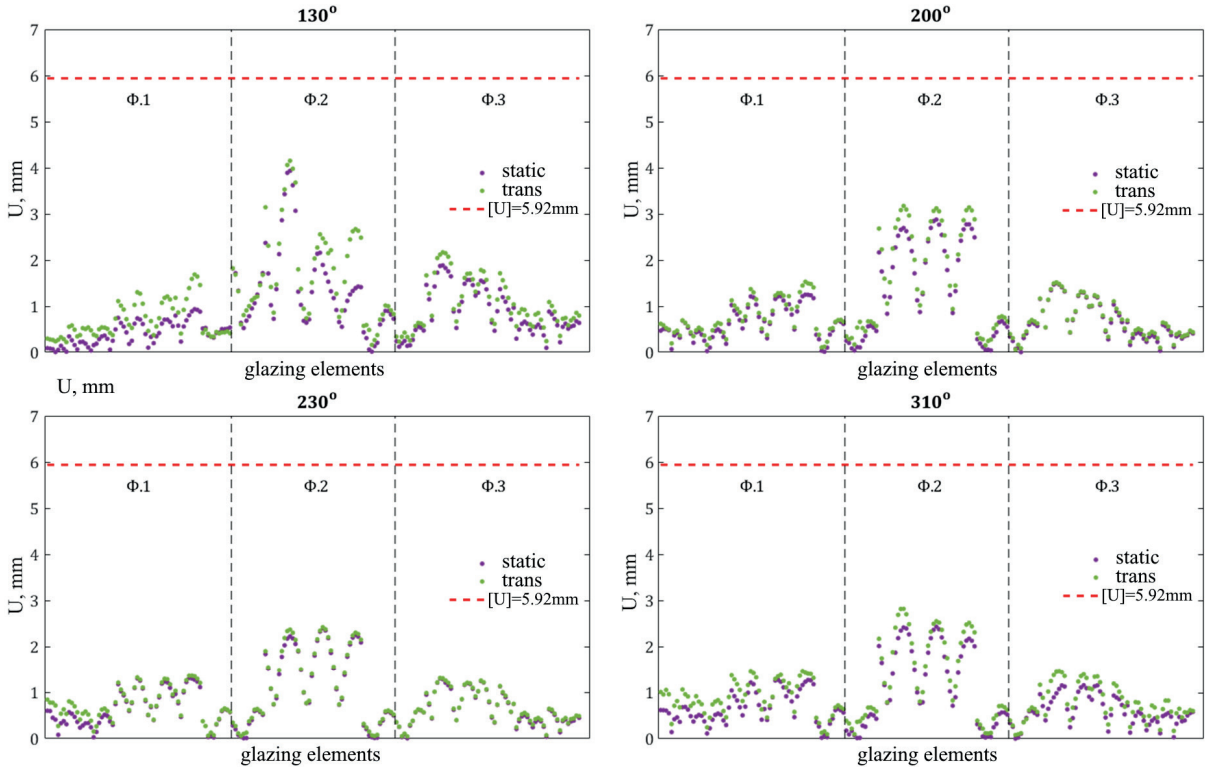

Figure 18. Flexures of glazing elements with limit value markings

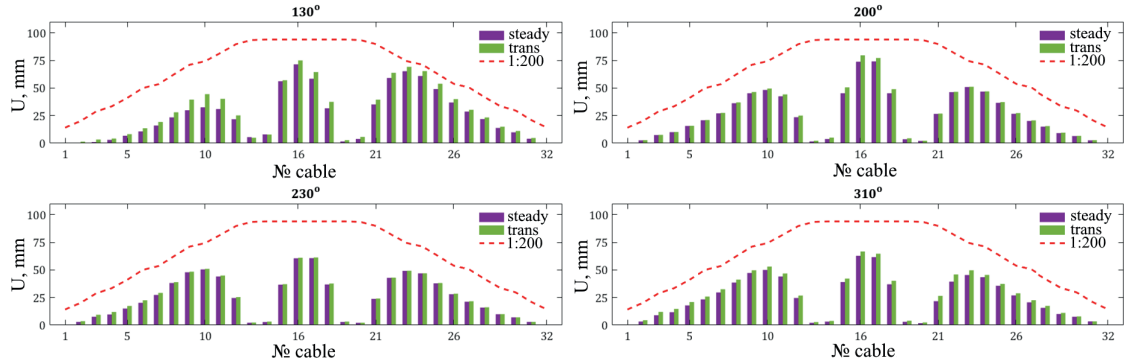

Figure 19. Maximum flexures of cables with limit value markings

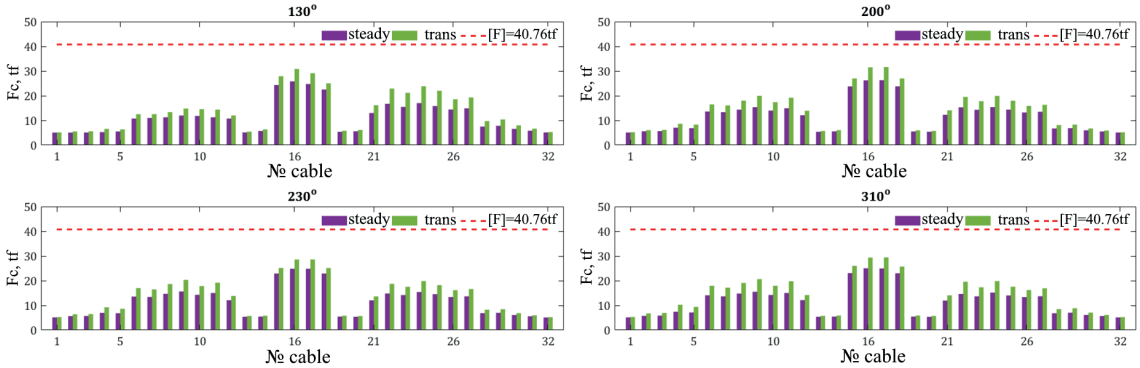

Figure 20. Maximum forces in cables with limit value markings

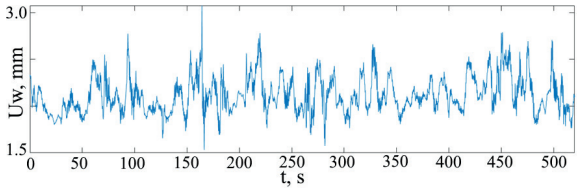

Figure 21. Flexures of a characteristic glazing element, mm (200°)

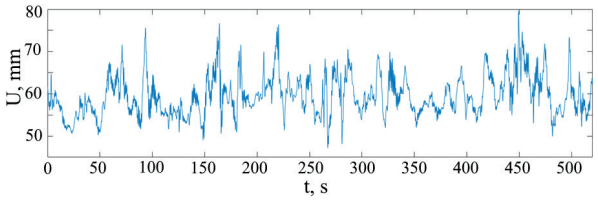

Figure 22. Flexures of a characteristic cable, mm (200°)

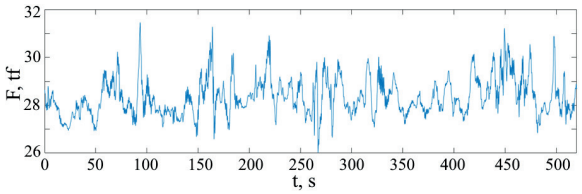

Figure 23. Forces in a characteristic cable, tf (200°)

Analysis of the results in Figs. 18-23 show that:

1. High-frequency resonance effects are periodically manifested under wind actions.
2. Presence of significant dynamic effects is revealed: flexures of glazing elements increased up to 2 times, flexures of cables to 40%, forces in cables to 40%.
3. The cable strength and façade stiffness do not exceed the criterion values even from the refined dynamic analysis.

3. CONCLUSIONS

The approach to the stress-strain state calculation of cable-stayed glass façades presented in this paper can be applied to any flexible structures.

It is shown that the application of nonlinear dynamic calculations allows to take into account the dynamic response to wind actions, which is the main one for flexible façade structures.

Numerical modelling of wind actions using LES turbulence model is a very costly approach and is often unavailable. Application of RANS models together with empirical methods (formulae 2-3) to determine hazardous wind directions and selective application of hybrid RANS-LES methods to determine design wind loads can reduce modelling time by orders of magnitude.

ACKNOWLEDGEMENTS

The research was funded by the National Research Moscow State University of Civil Engineering (grant for fundamental and applied scientific research, project No. 05-392/130).

REFERENCES

1. **Blocken B.** 50 years of computational wind engineering: past, present and future // J. Wind Eng. Wind Eng. Ind. Aerodyn., 2014, V. 129, pp. 69-102.
2. **Belostotsky A.M., Akimov P.A., Afanasyeva I.N..** Vychislitel'naya aerodinamika v zadachah stroitel'stva, Moscow: Izdatel'stvo ASV, 2017, 720 p. (in Russian).
3. **Cochran L., Derickson R.** A physical modeller's view of computational wind engineering // J. Wind Eng. Wind Eng. Ind. Aerodyn., 2011, V. 99, Issue 4, pp. 139-153.
4. **Meroney R.N., Derickson R.** Virtual reality in wind engineering: the windy world within the computer // J. Wind Eng. Wind Eng., 2014, V. 11, pp. 11-26.
5. **Thordal, M.S., Bennetsen, J.C., Capra, S., Koss, H.H.H..** Towards a standard CFD setup for wind load assessment of high-rise buildings: Part 1 - Benchmark of the CAARC building // Journal of Wind Engineering and Industrial Aerodynamics, 2020, V. 205, P. 104283.
6. **Bruno L. et al.** Codes and standards on computational wind engineering for structural design: State of art and recent trends // Wind and Structures, 2023, V., No. 2, pp. 37, No. 2, pp. 133-151.
7. CNR DT 207 R1/2018 Istruzioni per la valutazione delle azioni e degli effetti del vento sulle costruzioni, 2019. (in Italian)
8. ASCE/SEI 7-22 Minimum Design Loads and Associated Criteria for Building and other Structures, 2022.
9. Matematicheskoe (chislennoe)" modelirovanie vetrovyh nagruzok i vozdejstvii. Metodicheskoe posobie. Moscow: FAU "FCS", 2020, 61 p.
10. STO 02066523-089-1-2024 Numerical modelling of wind and snow actions, 2024
11. **Feng R.-q., Zhang L.-l., Wu Y., Shen S.-z.** Dynamic performance of cable net facades // Journal of Constructional Steel Research, 2009, V. 65, № 12. pp. 2217-2227.
12. **Feng R.-q., Ye J.-h., Wu Y., Shen S.-z.** Nonlinear response spectra of cable net facades // Soil Dynamics and Earthquake Engineering, 2012, V. 32, pp. 71-86.
13. **Feng R.-q., Ye J.-h., Wu Y., Shen S.-z.** Mechanical Behaviour of Glass Panels Supported by Clamping Joints in Cable Net Facades // Journal of Constructional Steel Research, 2012, V. 12, № 1. pp. 15-24.
14. **Amadio C., Bedon C.** Elastoplastic dissipative devices for the mitigation of blast resisting cable-supported glazing façades // Engineering Structures, 2012, V. 39, pp. 103-115.
15. **Bedon C., Amadio C**. Exploratory numerical analysis of two-way straight cable-net façades subjected to air blast loads // Engineering Structures, 2014, V. 79, pp. 276-289
16. **Yussof, M.M.** Cable-net supported glass façade systems. A thesis submitted in partial fulfilment for the degree of Doctor of Philosophy. United Kingdom, University of Surrey, 2015. P. 249
17. **Wang Y. et al.** Experimental and numerical studies on the static and the

dynamic behaviours of embedded cable support (ECS) glass facade system // Engineering Structures, 2019 V. 178, pp. 521-533.
18. **Xiang Y. et al.** Effect of the primary structure on the seismic response of the cable-net façade // Engineering Structures, 2020, V. 220, pp. 110989.
19. **Rizzo F., Bedon C.** Performance of cable-supported glass façades under time-depending wind action // Glass Structures & Engineering, 2023, V. 8, No. 1, pp. 81-98.
20. **Zhou Q. et al.** Frequency calculation method and wind-induced dynamic response of cable net façades considering the façade stiffness // Structures, 2023, V., V. 55, pp. 718-726.
21. **Menter F.R.** Review of the shear-stress transport turbulence model experience from an industrial perspective // J. Wind Eng. Wind Eng. Ind. Aerodyn., 2009, V. 23, pp. 305-316.
22. **Menter F., Hüppe A., Matyushenko A., Kolmogorov D**. An overview of hybrid RANS-LES models developed for industrial CFD // Appl. Sci., 2021, V. 11, p. 2459, 2021.
23. **Nicoud F., Ducros F.** Subgrid-scale stress modelling based on the square of the velocity gradient tensor // Flow, Turbulence and Combustion, 1999, V., No. 62, no. 62, №. 3, pp. 183-200.
24. **Menter F.R.** Best Practice: Scale-Resolving Simulations in ANSYS CFD. Version 2.00. Technical paper. ANSYS, 2015, 47 p.
25. **Goryachevsky O.S.** Numerical modelling of wind loads on windows // International Journal for Computational Civil and Structural Engineering, 2023, V. 19, No. 3, pp. 19, No. 3, pp. 114-129

СПИСОК ЛИТЕРАТУРЫ

1. **Blocken B.** 50 years of computational wind engineering: past, present and future // J. Wind Eng. Ind. Aerodyn., 2014, V. 129, pp. 69-102.
2. **Белостоцкий А.М., Акимов П.А., Афанасьева И.Н.** Вычислительная аэродинамика в задачах строительства, М.: Издательство АСВ, 2017, 720 с.
3. **Cochran L., Derickson R**. A physical modeler's view of computational wind engineering // J. Wind Eng. Ind. Aerodyn., 2011, V. 99, Issue 4, pp. 139-153.
4. **Meroney R.N., Derickson R**. Virtual reality in wind engineering: the windy world within the computer // J. Wind Eng., 2014, V. 11, pp. 11-26.
5. **Thordal, M.S., Bennetsen, J.C., Capra, S., Koss, H.H.H.** Towards a standard CFD setup for wind load assessment of high-rise buildings: Part 1 – Benchmark of the CAARC building // Journal of Wind Engineering and Industrial Aerodynamics, 2020, V. 205, P. 104283.
6. **Bruno L. et al.** Codes and standards on computational wind engineering for structural design: State of art and recent trends // Wind and Structures, 2023, V. 37, № 2, pp. 133-151.
7. CNR DT 207 R1/2018 Istruzioni per la valutazione delle azioni e degli effetti del vento sulle costruzioni, 2019. (in Italian)
8. ASCE/SEI 7-22 Minimum Design Loads and Associated Criteria for Building and other Structures, 2022.
9. Математическое (численное)" моделирование ветровых нагрузок и воздействий. Методическое пособие, М.: ФАУ «ФЦС», 2020, 61 с.
10. СТО 02066523-089-1-2024 Численное моделирование ветровых и снеговых воздействий, НИУ МГСУ, НИЦ СтаДиО, 2024
11. **Feng R.-q., Zhang L.-l., Wu Y., Shen S.-z.** Dynamic performance of cable net facades // Journal of Constructional Steel Research, 2009, V. 65, № 12. pp. 2217-2227.
12. **Feng R.-q., Ye J.-h., Wu Y., Shen S.-z**. Nonlinear response spectra of cable net

facades // Soil Dynamics and Earthquake Engineering, 2012, V. 32, pp. 71-86.
13. **Feng R.-q., Ye J.-h., Wu Y., Shen S.-z.** Mechanical Behavior of Glass Panels Supported by Clamping Joints in Cable Net Facades // Journal of Constructional Steel Research, 2012, V. 12, № 1. pp. 15-24.
14. **Amadio C., Bedon C.** Elastoplastic dissipative devices for the mitigation of blast resisting cable-supported glazing façades // Engineering Structures, 2012, V. 39, pp. 103-115.
15. **Bedon C., Amadio C.** Exploratory numerical analysis of two-way straight cable-net façades subjected to air blast loads // Engineering Structures, 2014, V. 79, pp. 276–289
16. **Yussof, M.M.** Cable-net supported glass façade systems. A thesis submitted in partial fulfilment for the degree of Doctor of Philosophy. United Kingdom, University of Surrey, 2015. P. 249
17. **Wang Y. et al.** Experimental and numerical studies on the static and the dynamic behaviors of embedded cable support (ECS) glass facade system // Engineering Structures, 2019 V. 178, pp. 521-533.
18. **Xiang Y. et al.** Effect of the primary structure on the seismic response of the cable-net façade // Engineering Structures, 2020, V. 220, pp. 110989.
19. **Rizzo F., Bedon C**. Performance of cable-supported glass façades under time-depending wind action // Glass Structures & Engineering, 2023, V. 8, № 1, pp. 81-98.
20. **Zhou Q. et al.** Frequency calculation method and wind-induced dynamic response of cable net façades considering the façade stiffness // Structures, 2023, V. 55, pp. 718-726.
21. **Menter F.R.** Review of the shear-stress transport turbulence model experience from an industrial perspective // J. Wind Eng. Ind. Aerodyn., 2009, V. 23, pp. 305-316.
22. **Menter F., Hüppe A., Matyushenko A., Kolmogorov D.** An overview of hybrid RANS–LES models developed for industrial CFD // Appl. Sci., 2021, V. 11, p. 2459, 2021.
23. **Nicoud F., Ducros F.** Subgrid-scale stress modelling based on the square of the velocity gradient tensor // Flow, turbulence and Combustion, 1999, V. 62, №. 3, pp. 183-200.
24. **Menter F.R.** Best Practice: Scale-Resolving Simulations in ANSYS CFD. Version 2.00. Technical paper. ANSYS, 2015, 47 p.
25. **Горячевский О.С.** Численное моделирование ветровых давлений на окна. Валидация для типового многоэтажного здания квадратной формы // International Journal for Computational Civil and Structural Engineering, 2023, Т. 19, № 3, с. 114-129

Oleg Sergeevich Goryachevsky – Deputy Director at A.B. Zolotov REC CM of the National Research Moscow State University of Civil Engineering; 129337, Russia, Moscow, Yaroslavskoe shosse, 26.
E-mail: osgoryachevskij@mail.ru

Олег Сергеевич Горячевский – заместитель директора НОЦ КМ им. А.Б. Золотова Национального исследовательского Московского государственного строительного университета; 129337, Россия, г. Москва, Ярославское шоссе, д. 26.
E-mail: osgoryachevskij@mail.ru

Alexander Mikhailovich Belostotsky – DSc, Professor, Full Member of the Russian Academy of Architecture and Construction Sciences. Scientific adviser at A.B. Zolotov REC CM of the National Research Moscow State University of Civil Engineering; 129337, Russia, Moscow, Yaroslavskoe shosse, 26.
E-mail: amb@stadyo.ru

Александр Михайлович Белостоцкий – Научный руководитель НОЦ КМ им. А.Б. Золотова Национального исследовательского Московского государственного строительного университета; 129337, Россия, г. Москва, Ярославское шоссе, д. 26.
E-mail: amb@stadyo.ru